

Article

Electronic Properties, Linear and Nonlinear Performance of KAgCh ($Ch = S, Se$) Compounds: A First-Principles Study

Taieb Seddik ¹, Debidatta Behera ², Mohammed Batouche ¹, Walid Ouerghui ³, Houda Ben Abdallah ³, Ram Krishna Sarkar ⁴, Mostafa M. Salah ^{5,*}, Ahmed Shaker ⁶ and Sanat Kumar Mukherjee ^{2,*}

¹ Laboratory of Quantum Physics of Matter and Mathematical Modeling (LPQ3M), Mascara University, Mascara 29000, Algeria; sedik_t@yahoo.fr (T.S.); batouchemohammed@yahoo.fr (M.B.)

² Department of Physics, Birla Institute of Technology, Mesra, Ranchi 835215, India; debidatta95@yahoo.com

³ Laboratoire de Physique de la Matière Condensée, Département de Physique, Faculté des Sciences de Tunis, Université Tunis El Manar, Tunis 2092, Tunisia; ouerghuiwalid@yahoo.fr (W.O.); houdabenabdallah18@gmail.com (H.B.A.)

⁴ Department of Physics, Birla Institute of Technology (Mesra), Off-Campus Deoghar, Jasidih, Deoghar 814142, India; ramkrishnabit@gmail.com

⁵ Electrical Engineering Department, Future University in Egypt, Cairo 11835, Egypt

⁶ Faculty of Engineering, Ain Shams University, Cairo 11535, Egypt; ahmed.shaker@eng.asu.edu.eg

* Correspondence: mostafa.abdulkhaled@fue.edu.eg (M.M.S.); sanat_aphy@yahoo.co.in (S.K.M.)

Abstract: In the current study, the peculiar nonlinear optical (NLO) properties of KAgCh ($Ch = S, Se$) and their structural, electronic, and thermodynamic properties are computed utilizing the FP-LAPW (full-potential linearized augmented plane wave) approach as embedded in Wein2K code. The Perdew–Burke–Ernzerh of generalized gradient approximation (PBE-GGA) was considered for the structural optimization. The computed bandgaps are found to be 2.57 and 2.39 eV for KAgS and KAgSe, respectively. Besides the structural and electronic properties, we also computed the refractive indices $n(\omega)$, surface energy loss function (SELF), and nonlinear optical susceptibilities. The estimated refractive indices, energy band gap, and their frequency dependence for the investigated KAgCh ($Ch = S, Se$) compounds, along with the NLO coefficients, are found to be in good agreement with the earlier reports. These current findings suggest that KAgCh ($Ch = S, Se$) can be recommended for nonlinear optical applications in the near-infrared spectrum.

Keywords: nonlinear optical compounds; density functional theory; electronic properties; nonlinear refractive index; surface energy loss function (SELF)

1. Introduction

Extensive research studies have been carried out in the last several years to develop various types of new inorganic and organic nonlinear optical (NLO) compounds. These NLO compounds display promising applications for optical parametric oscillation or amplification via second-harmonic generation, sum and difference frequency mixing, and as efficient photonic devices [1–6]. Therefore, exceptionally efficient NLO crystals must be developed for usage in the visible, ultra-violet, and deep ultraviolet range in order to perform laser processing and laser spectroscopy, such as laser tailoring of molecules and optical triggering [7–10]. Ternary alkali metal chalcogenides with the general formula ABCh, where A represents alkali metals such as Na, K, and Rb; B represents Cu and Ag; and Ch is a chalcogen (S, Se, and Te), have recently attracted the interest of materials researchers [11–16]. NaCuCh and KCuCh ($Ch = S, Te$) were the first alkali metal chalcogenides to be explored that have PbFCl and Ni₂In-type structures [16]. Later on, G. Savelsberg and H. Schäfer [10] explored the new KAgSe compounds, finding that this material adopts a tetragonal PbFCl-type structure with space group P4/nmm (#129). This was followed by a theoretical analysis of its electronic band structure, dynamical



Citation: Seddik, T.; Behera, D.; Batouche, M.; Ouerghui, W.; Abdallah, H.B.; Sarkar, R.K.; Salah, M.M.; Shaker, A.; Mukherjee, S.K. Electronic Properties, Linear and Nonlinear Performance of KAgCh ($Ch = S, Se$) Compounds: A First-Principles Study. *Crystals* **2023**, *13*, 726. <https://doi.org/10.3390/cryst13050726>

Academic Editor: Ludmila Isaenko

Received: 26 March 2023

Revised: 12 April 2023

Accepted: 14 April 2023

Published: 25 April 2023



Copyright: © 2023 by the authors. Licensee MDPI, Basel, Switzerland. This article is an open access article distributed under the terms and conditions of the Creative Commons Attribution (CC BY) license (<https://creativecommons.org/licenses/by/4.0/>).

behavior, and elastic attributes [8]. Assuming that both KAgS and KAgTe are analogues to KAgSe compound, a theoretical study on structural and thermodynamic stability as well as electronic and elastic properties has been carried out [17,18]. Aside from their properties as 2D materials, KAgCh have a number of notable behaviors, including an ideal direct band gap, impressive optical absorption in the visible light region, significant carrier mobilities, and remarkable performances in the corresponding thermoelectric and photovoltaic nano-devices [9,15–22]. The effect of nonlinearity can also be seen in different types of beam propagation, leading to soliton formation, breather formation, and soliton–breather pair formation [23–32].

Despite a few notable experimental contributions, we still know relatively little about the electronic and optical characteristics of these KAgCh ($Ch = S, Se$) ternary alkali metal chalcogenides, which will be crucial for their use in technological applications. Further theoretical research into such properties is thus desired. Motivated by this purpose, we conducted a comprehensive study on the linear and nonlinear optical performance of KAgCh ($Ch = S, Se$) compounds, which has not been performed by any research group till now to the best of our knowledge. The structural, electronic optical, and thermodynamic properties of KAgCh ($Ch = S, Se$) compounds are reported in this paper. The three portions of the manuscript include the introduction, a full description of the computational approach adopted in the study, and the results and conclusions determined to be of major value to the field of current investigations.

2. Computational Method

The quantum mechanically focused calculations in the present work were performed using the Wien2K code [33] implementation of density functional theory (DFT) [20,34–37] based on the full-potential linearized augmented plane wave (FP-LAPW) strategy [21]. For the structural optimization, the GGA-PBE approach [22] was considered in conjunction with Tran–Blaha modified Becke–Johnson potential (TB-mBJ) [38] to assess the electronic and optical properties of the investigated compounds. A cut-off value for $R_{MTv} \times K_{MAX}$ of 9.0 is considered in this study. The term K_{MAX} represents the largest selected value of the reciprocal lattice vectors utilized to extend the plane wave, while R_{MT} stands for the muffin tin (MT) radius of the smallest atomic sphere [39]. The simulations used a self-consistent precision of total energy of 10^{-4} Ry. The MT atomic spheres R_{MT} have radii of 2.03, 2.31, 2.50, and 2.65 a.u. for K, Ag, S, and Se atoms, respectively. The charge density and potential were extended up to $G_{max} = 12$ a.u. $^{-1}$. Using the modified tetrahedron approach, a dense mesh of $17 \times 17 \times 10$ uniformly distributed k-points was employed inside the Brillouin zone (BZ) [40,41], where the total energy concentration is set up to 10^{-6} Ry. We used the Gibbs2 code [42] to solve the Gibbs function within the quasi-harmonic Debye model to obtain the thermodynamic characteristics of KAgCh ($Ch = S, Se$) compounds. At temperatures between 0 and 1000 K and pressures between 0 and 8GPa, the thermal effects of KAgCh ($Ch = S, Se$) were examined. Furthermore, utilizing the Vienna Ab-initio Simulation Package (VASP) [43], we performed the phonon dispersion study in order to study the dynamical stability of the investigated KAgCh ($Ch = S, Se$).

3. Results and Discussion

3.1. Structural Properties

As shown in Figure 1, the investigated KAgCh ($Ch = S, Se$) exists in the tetragonal crystal structure [10], where the K, Ag, and Ch atoms are located at specific positions at $(1/4, 1/4, 0.657)$, $(3/4, 1/4, 0)$, and $(1/4, 1/4, w)$, respectively. Accordingly, both KAgS and KAgSe compounds are relaxed and optimized to obtain the ground state parameters. Table 1 includes the optimized structural parameters and experimental results for comparison [10,17].

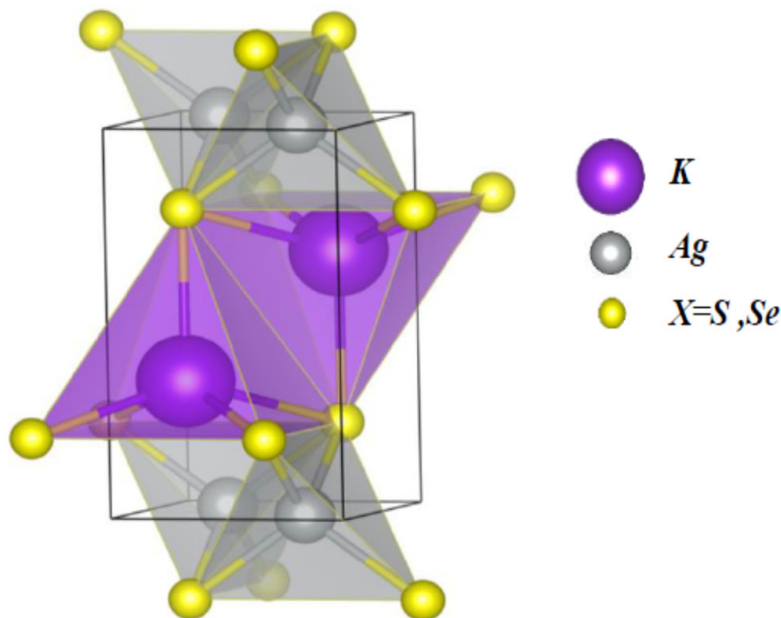


Figure 1. Crystal structure of KAgCh ($Ch = S, Se$) using VESTA [26].

Table 1. Lattice parameters (\AA), c/a ratio, bulk modulus B (GPa), its derivative B' , and formation energy E_f (eV) for KAgCh ($Ch = S, Se$).

		$a = b$	c	c/a	B	B'	z_K	w_{Ch}	E_f
KAgS	This work	4.39	7.56	1.72	39.14	4.41	0.657	0.216	-0.71
	Expt.	4.391 [44]	7.556 [44]						
	Other works	4.42 [17]	7.53 [17]	1.70 [17]	29.96 [17]	6.61 [17]			
		4.32 [17]	7.36 [17]		34.79 [17]	7.18 [17]			
KAgSe	This work	4.51	7.72	1.71	35.37	5.00	0.654	0.231	-0.61
	Expt. [10]	4.52	7.59	1.68			0.6579	0.2156	
		4.29 [44]	7.275 [44]						
	Other works	4.56 [11]	7.77 [11]	1.70 [11]	25.87 [17]	6.47 [17]			
		4.57 [17]	7.79 [17]		30.03 [17]	6.99 [17]			
		4.47 [17]	7.61 [17]						

From Table 1, it is remarked that our obtained lattice parameters are in decent agreement with other reported experimental and theoretical works. Besides, it is remarked that the bulk modulus decreases when going from S to Se, which is principally due to the difference in atomic radius. Furthermore, to know the stability of the studied KAgCh ($Ch = S, Se$) materials, we computed the formation energy (E_f):

$$E_f(\text{KAgCh}) = (E_T(\text{KAgCh}) - [E_K + E_{Ag} + E_{Ch}]) \quad (1)$$

where $E_T(\text{KAgCh})$ is the total energy and E_K , E_{Ag} , and E_{Ch} are the energies of K, Ag, and Ch (S/Se) atoms, respectively. The computed E_f for KAgCh ($Ch = S, Se$) is found to be -0.71 eV/atom and -0.67 eV/atom, respectively. This negative value suggests the formability of the researched KAgCh ($Ch = S, Se$) compounds [45]. The phonon spectra are computed using the finite displacement approach in the Vienna Ab-initio Simulation Package (VASP). The phonon dispersion in the first Brillouin zone was calculated along high symmetry directions (M-K- Γ -A-L) (Figure 2). The real and imaginary frequencies in the phonon plot for positive and negative frequencies are used to signify the balanced and unbalanced phonon structures, respectively. The lack of an imaginary frequency at the Γ -point attests to the examined KAgCh ($Ch = S, Se$) compounds' dynamical stability [46,47]. The obtained results agree with other reports.

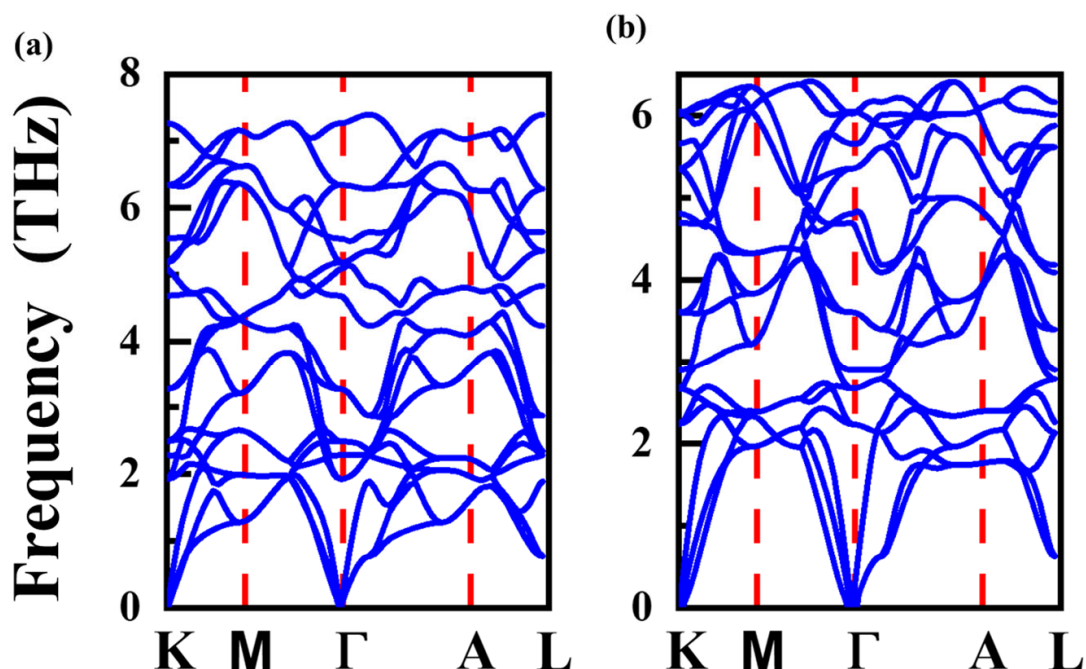


Figure 2. Phonon dispersion spectrum for (a) KAgS and (b) KAgSe.

3.2. Electronic Properties

Calculating the electronic band structure is necessary to comprehend the physical properties of a crystalline solid, which almost entirely describe optical and transport aspects [48,49]. In the k -space, we computed the electronic band structure for KAg Ch ($Ch = S, Se$) compounds for the high symmetry points in the irreducible Brillouin zone, as displayed in Figure 3a–d. The GGA-PBE potential notably underestimates the band gap of a material, while the TB-mBJ approximation [38,50] may forecast band gaps that are comparable to experimental values. In this investigation, two distinct exchange correlation functionals, the GGA-PBE and TB-mBJ functionals, were used to evaluate the electronic band structures of KAg Ch ($Ch = S, Se$). Figure 3a–d shows that the band gaps of the KAg Ch ($Ch = S, Se$) compounds are direct and are located at Γ point. The calculated direct band gaps by GGA-PBE and TB-mBJ functionals are 1.02 eV and 2.57 eV for KAgS and 1.03 eV and 2.39 eV for KAgSe, respectively. The computed bandgaps obtained with GGA-PBE are in accordance with other reported theoretical results; however, the values obtained by TB-mBJ are different to those estimated by M.A. Mahmoud [17], thus more investigation on the band structure calculation is needed. We also calculated the effective mass [40,51] of electrons and holes using the following relationship:

$$m^* = \hbar^2 \left(\frac{\partial^2 E}{\partial^2 k} \right)^{-1} \quad (2)$$

The effective masses of electrons are approximately 0.70 and 0.63, while the effective masses of holes are 0.37 and 0.32 for KAgS and KAgSe, respectively.

The density of states (DOS) computation can be used to better clarify how distinct atomic states contribute to the band structure [41,52]. The amount of accessible electronic states per unit energy per unit volume is generally referred to as the DOS [39]. Figure 4a,b illustrates the total and partial DOS of KAg Ch ($Ch = S, Se$) materials. From this figure, one can notice that the valence band maximum is occupied principally by the Ag-d and Ch -s states, while the lowest conduction band is formed by Ag-s and s,p orbitals for Ch atoms. Additionally, a strong hybridization between Ag-d states and Ch -s states indicates a covalent character of the Ag- Ch bond.

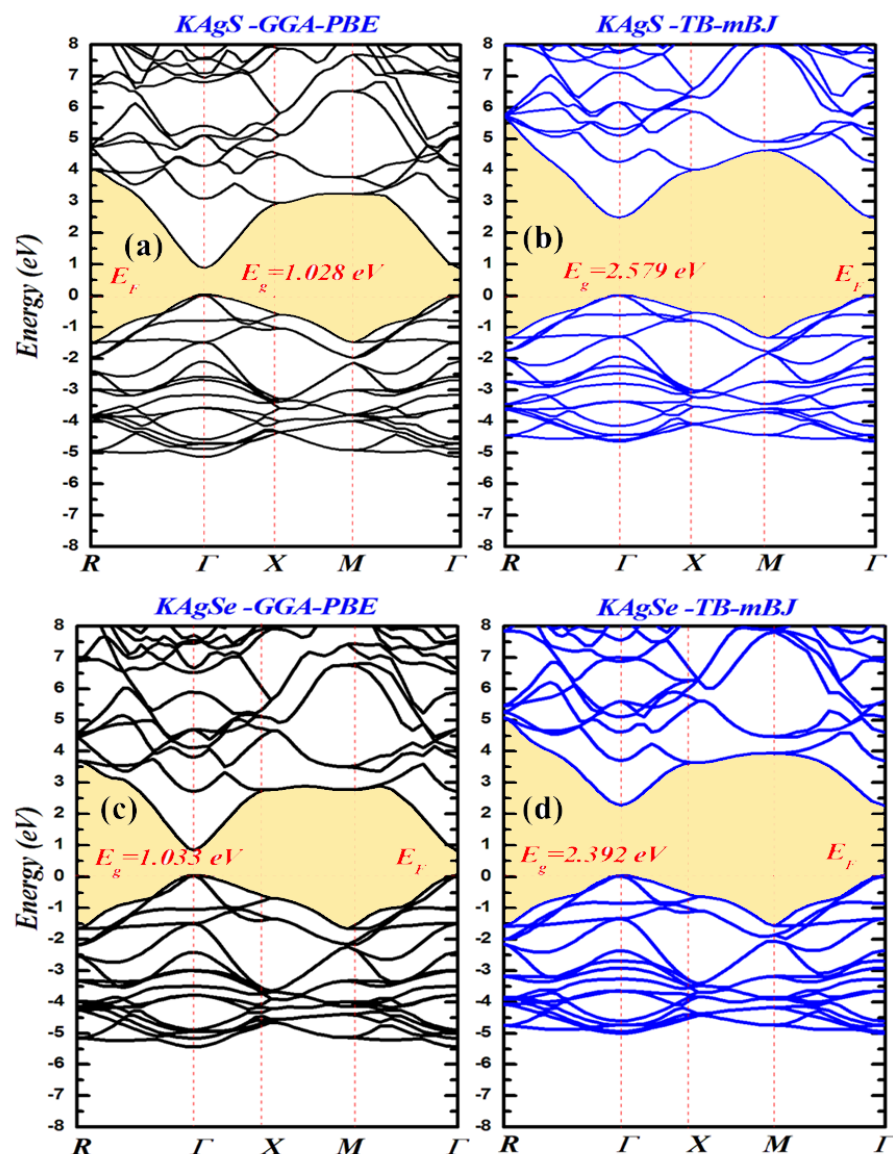


Figure 3. (a–d) Computed band structure for KAgCh ($Ch = S, Se$) employing different exchange correlation functionals.

3.3. Thermodynamic Properties

The quasi-harmonic Debye approximation is used in this study to examine the thermodynamic properties of KAgCh ($Ch = S, Se$). The specific heat at a constant volume and pressure (C_v and C_p), thermal expansion (α), and Debye temperature (θ_D) were calculated in the pressure range 0–8 GPa. The quasi-harmonic Debye model was demonstrated to perform well for temperatures between 0 K and 1000 K. Figures 5a and 6a display graphically how the temperature and pressure affect the specific heat capacity (C_V) for KAgCh ($Ch = S, Se$). Upon comparing the C_V diagrams of the two compounds, it can be seen that C_V increases linearly up to 300 K. When temperatures are between 300 K and 700 K, it increases more slowly, and when temperatures are beyond 700 K, C_V is almost constant. According to the well-known Debye model, C_V is expected to rise at low temperatures. This can be explained by functioning of long-wavelength vibration modes of the lattice and, if the lattice is considered as a continuum, it is possible to approach these modes [53]. However, as suggested by Petit and Dulong's law [54], at significantly high temperatures, the classical behavior ($C_V(T) \propto 3R$ for mono-atomic materials) is observed. For KAgCh ($Ch = S, Se$), the computed values of C_V at 300 K (0 GPa) were discovered to be $67 \text{ J mol}^{-1} \text{ K}^{-1}$ and $68 \text{ J mol}^{-1} \text{ K}^{-1}$, respectively.

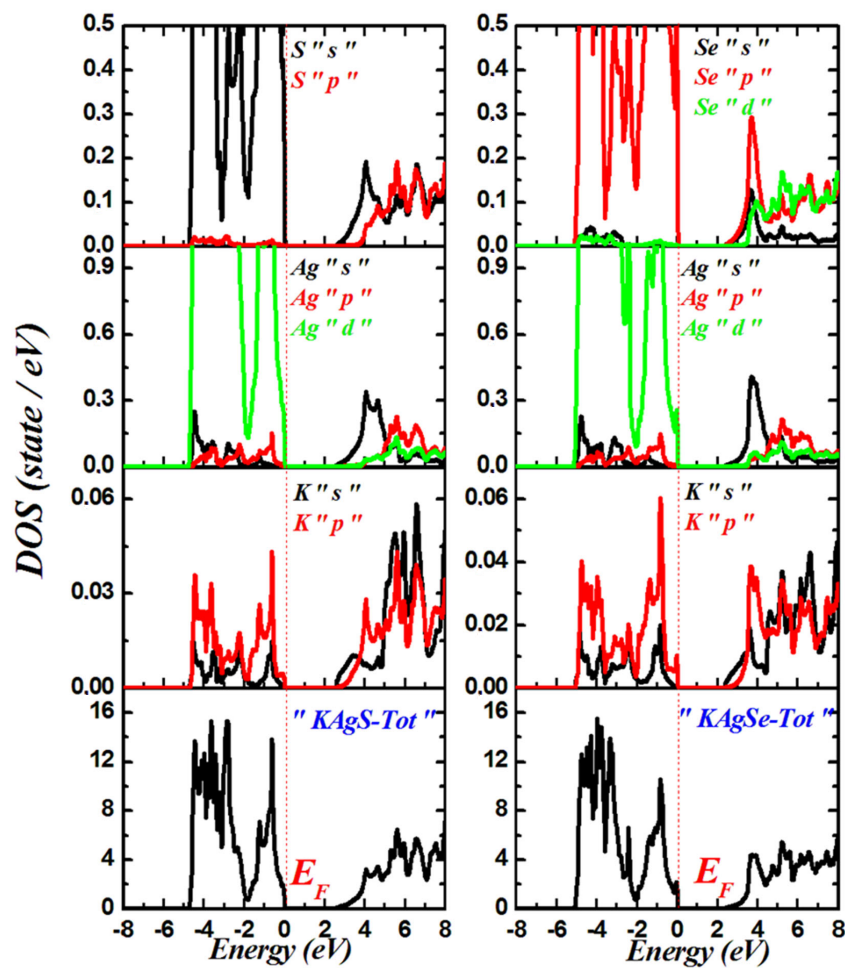


Figure 4. (a,b) Computed density of states for KAgCh ($\text{Ch} = \text{S}, \text{Se}$) employing TB-mBJ exchange correlation functionals.

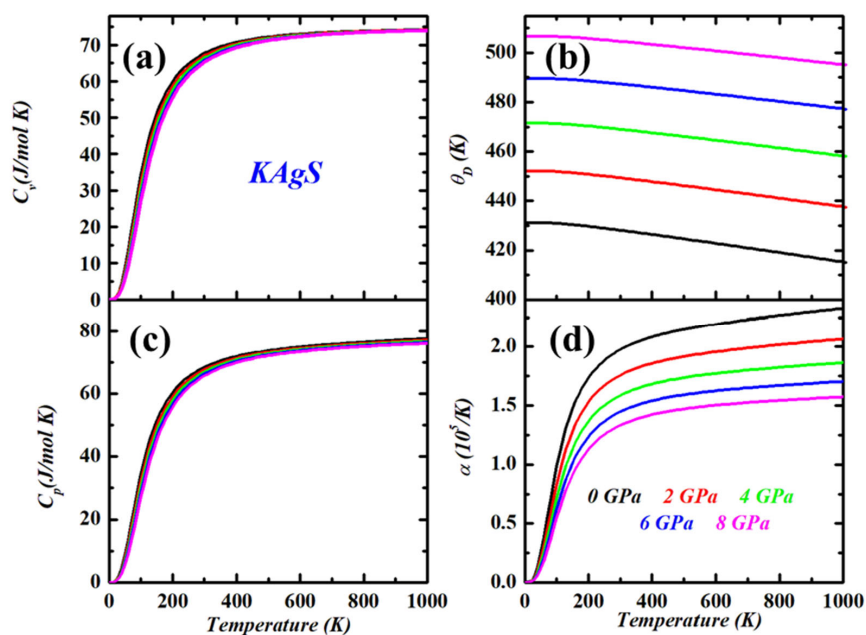


Figure 5. (a–d) Variation of different thermodynamic parameters with temperature (0–1000 K) and pressure (0–8 GPa) for KAgS .

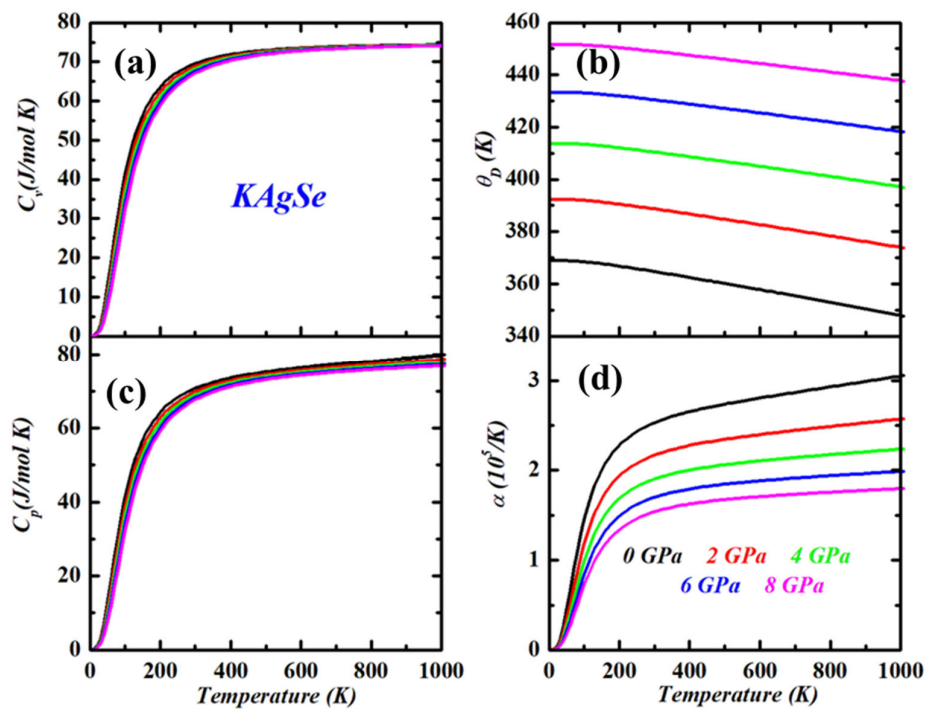


Figure 6. (a–d) Variation in different thermodynamic parameters with temperature (0–1000 K) and pressure (0–8 GPa) for KAgSe.

According to Figures 5b and 6b, it is shown that both pressure and temperature affect the Debye temperature (θ_D) [55] of KAgCh ($Ch = S, Se$). It is obvious when comparing the two plots that the value of θ_D falls very gradually, but achieves a constant value over a range of temperature and pressure. For both substances, it decreases with the increasing temperature at a pressure of 0 GPa. At a particular temperature, it is seen that the value of θ_D increases with pressure. The computed values of θ_D for KAgCh ($Ch = S, Se$) at a pressure of 0 GPa and ambient temperature are 428 and 367 K, respectively.

Further, Figures 5c and 6c display the heat capacity C_p variation with pressure and temperature. As the temperature rises, the variation characteristics of C_p values, which are similar to those of C_v at lower temperatures, become more evident. On the other hand, when the temperature is high, the behavior of C_p is found to be different from C_v . With the increase in pressure, C_p decreases without converging to a single value. There is a noticeable increase in the heat capacity as the temperature rises.

Moreover, Figures 5d and 6d display the variation in the thermal expansion coefficient (α) with changing temperature and pressure. It is relatively simple to demonstrate using these data that the value increases linearly and gradually at high temperatures, but abruptly above 300 K. This can be observed by comparing the two sets of data. The saturation of up to 300 K may be the reason for this trend. KAgS was calculated to have a value of 1.92×10^{-5} per Kelvin, while KAgSe has a value of 1.97×10^{-5} per Kelvin at a pressure of 0 GPa and ambient temperature. Pressure has been discovered to have the potential to lower this value [56]. The influence of pressure on the value, however, becomes more pronounced and diminishes more quickly as the temperature rises. This is because of the fact that the quasi-harmonic model performs poorly in conditions of both high temperature and low pressure.

3.4. Optical Properties

3.4.1. Linear Optical Property

We estimated that the optical characteristics of KAgCh ($Ch = S, Se$) subject to photon energy are significant for applications in optoelectronic devices. TB-mBJ functional was used to calculate all of the parameters. Because of the functional inaccurate prediction of

the energy band gap with the GGA-PBE, it was ignored. Figure 7a,b shows the predicted optical characteristics of KAgCh ($Ch = S, Se$) for a photon energy up to 12 eV. The hexagonal structure of KAgCh ($Ch = S, Se$) enables us to determine the associated properties for two polarization directions ($E \parallel x$ and $E \parallel z$). In order to analyze the optical response of a medium and its dispersive behavior at all photon energies, we determined the real (ϵ_1) and the imaginary (ϵ_2) parts of the dielectric function of KAgS and KAgSe, which are displayed in Figure 7a,b. The static dielectric constant $\epsilon_1(0)$ reflects the dielectric response at the zero-frequency limit [57]. All of the obtained values of the static dielectric constant are listed in Table 2. From Table 2, it can be deduced that the highest static dielectric constant is obtained in the case of the KAgCh ($Ch = S, Se$) compounds in the direction of polarization $E \parallel z$.

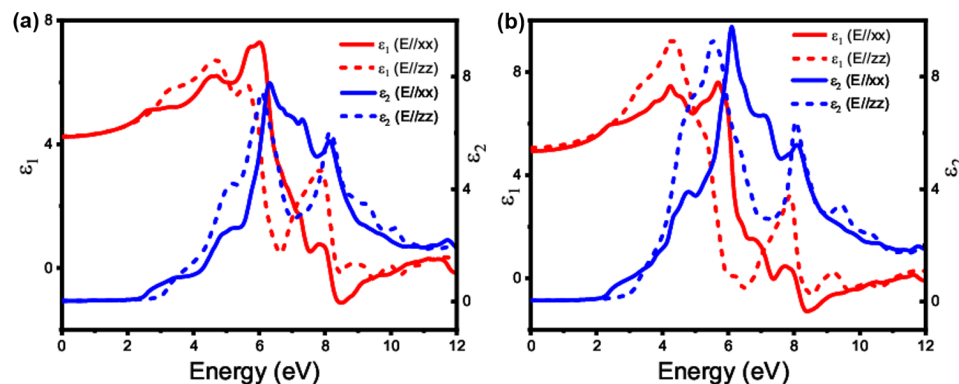


Figure 7. Calculated real and imaginary parts of the dielectric function of (a) KAgS and (b) KAgSe.

Table 2. Calculated optical constants for KAgS and KAgSe: static dielectric constant $\epsilon_1(0)$, static refractive index $n(0)$, oscillator energy E_0 , dispersion energy E_d , and oscillator strength \mathcal{F} .

Compound	$\epsilon_1(0)$ (E//x)	$\epsilon_1(0)$ (E//z)	$n(0)$ (E//x)	$n(0)$ (E//z)	E_0 (eV) (E//x)	E_0 (eV) (E//z)	E_d (eV) (E//x)	E_d (eV) (E//z)	\mathcal{F} (eV ²) (E//x)	\mathcal{F} (eV ²) (E//z)
KAgS	4.24	4.25	2.05	2.06	6.28	6.40	20.36	20.82	128.02	133.32
KAgSe	4.93	5.06	2.22	2.24	5.75	5.98	22.64	24.03	130.36	143.72

A transition between the occupied states at the upper valence band and the unoccupied at the occupied at the conduction band minimum is considered to be the origin of the major absorption peak shown in the $\epsilon_2(\omega)$ curve, which is positioned at about 206 nm (6 eV) [48,58–60]. It should be remarked from Figure 8 that the extinction coefficient curve $k(\omega)$ and the imaginary portion of the dielectric function $\epsilon_2(\omega)$ exhibit behavior that is comparable.

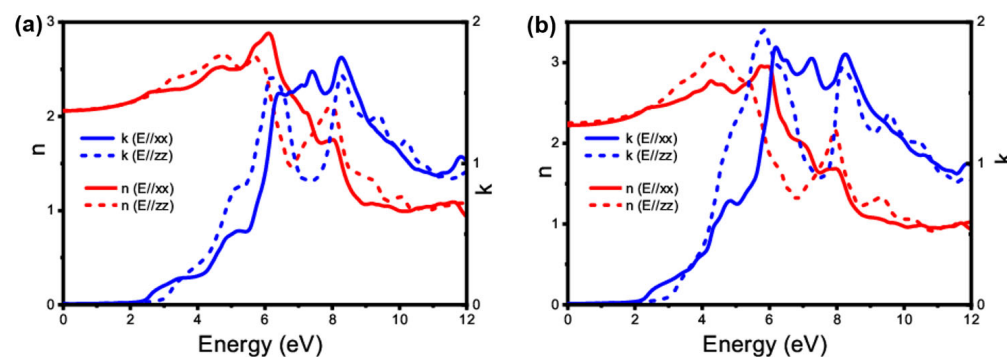


Figure 8. Computed complex refractive index $n(\omega)$ and extinction coefficient $k(\omega)$ of (a) KAgS and (b) KAgSe.

Next, Figure 8 shows the spectral dependence of the refractive index on the photon energy. It can be observed that the $n(\omega)$ curves have high values at low frequencies, which decrease significantly towards higher frequencies. At low optical frequencies, the Wemple–DiDomenico (WDD) single oscillator model is commonly used to analyze the refractive index. The WDD model is given by the following relation:

$$(n^2 - 1)^{-1} = \frac{E_0}{E_d} - \frac{1}{E_0 E_d} (h\nu)^2 \quad (3)$$

where E_d and E_0 denote the dispersion of the electronic dielectric function and the single oscillator energy, respectively. From the low-frequency region, by fitting the plot $(n^2 - 1)^{-1}$ versus $(h\nu)^2$, we can estimate the dispersion parameters and the single oscillator energies for KAgS and KAgSe. Figure 9 illustrates the spectral dependence of the $(n^2 - 1)^{-1}$ versus $(h\nu)^2$ for both KAgS and KAgSe compounds. A crucial parameter given by the WDD model is the oscillator strength found from $\mathcal{F} = E_0 E_d$. The values of E_d and E_0 and \mathcal{F} are reported in Table 2. Once the values E_0 and E_d are calculated, the determination of the static refractive index (n_0) is deduced using the following relation [61]:

$$n_0 = \left(1 + \frac{E_d}{E_0} \right)^{1/2} \quad (4)$$

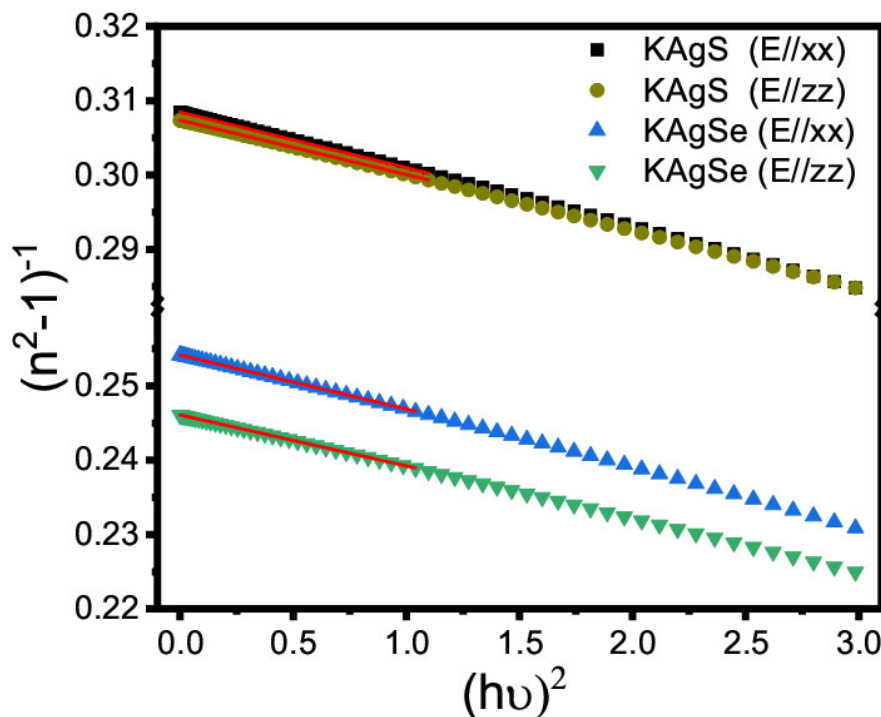


Figure 9. $(n^2 - 1)^{-1}$ versus $(h\nu)^2$ for $\sigma(\omega)$ of KAgS and KAgSe.

All simulated static refractive indexes $n(0)$ for KAgS and KAgSe compounds are given in Table 2. The obtained values of static refractive index obey the relation $n(0) = \varepsilon_1^{1/2}(0)$.

The photon-energy-dependent absorption coefficient of KAgCh ($Ch = S, Se$) is shown in Figure 10. It is important to take note of the several peaks in this absorption spectra caused by the interband transitions from the bonding band to the anti-bonding band [62]. The maximum absorptions are observed in the UV range for the KAgSe compound along the E//z polarization direction. In the visible range, all compounds under study show very low absorptions, which indicates high transmittance of light.

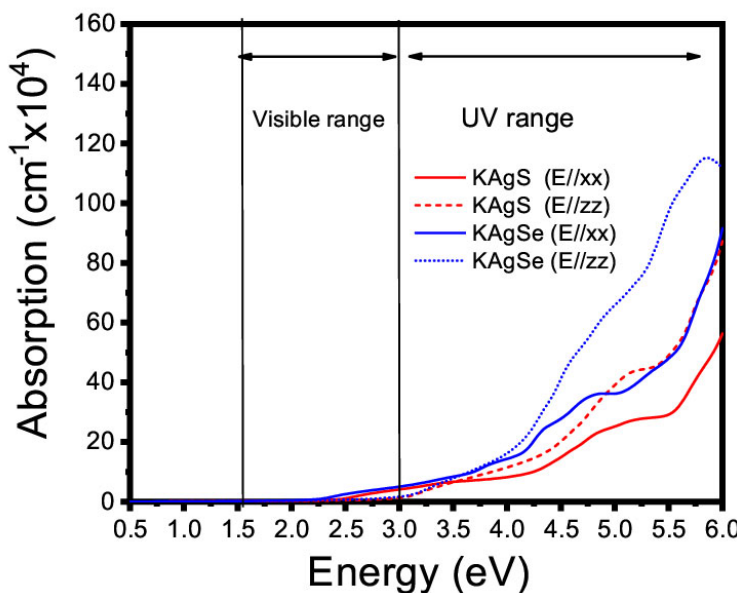


Figure 10. Calculated absorption coefficient $\alpha(\omega)$ of KAgCh (Ch = S, Se).

By definition, $L(\omega)$ is the surface energy loss function describing the energy loss of a fast electron crossing a medium and for the determination of plasmon frequency [45,63–65]. The calculated surface energy loss function (SELF $L(\omega)$) spectra for KAgS and KAgSe are presented in Figure 11.

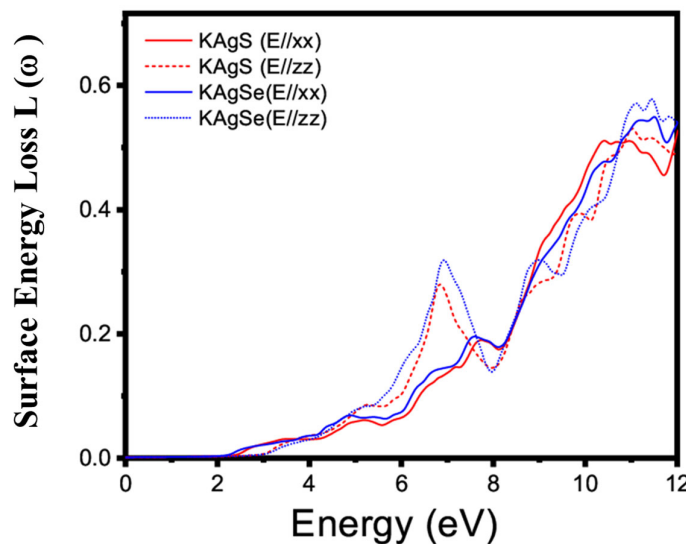


Figure 11. Simulated surface energy loss function $L(\omega)$ of KAgS and KAgSe.

In addition, the surface energy loss function (SELF) represents the energy loss of fast electrons crossing the surface of the material and can be evaluated by the following relation [66]:

$$\text{SELF} = -\text{Im}\left(\frac{1}{\varepsilon + 1}\right) = \frac{\varepsilon_2}{(\varepsilon_1 + 1)^2 + \varepsilon_2^2} \quad (5)$$

The electron energy loss takes on relatively low values for energies below 6 eV. Beyond 3 eV, energy that coincides with the peak of the absorption observed in $\varepsilon_2(\omega)$ spectrum, the electron energy loss increases. The characteristic behavior of the dielectric depends not only on its constitutive parameters, but also on the energy.

The electron conduction process produced in the material is described by the optical conductivity, which is calculated using the following relation [66]:

$$\sigma_{opt} = \frac{\alpha n c}{4\pi} \quad (6)$$

We notice, according to Figure 12, an increase in conductivity going from the visible to the UV range, with a gradual increase for KAgSe material in the x polarization direction.

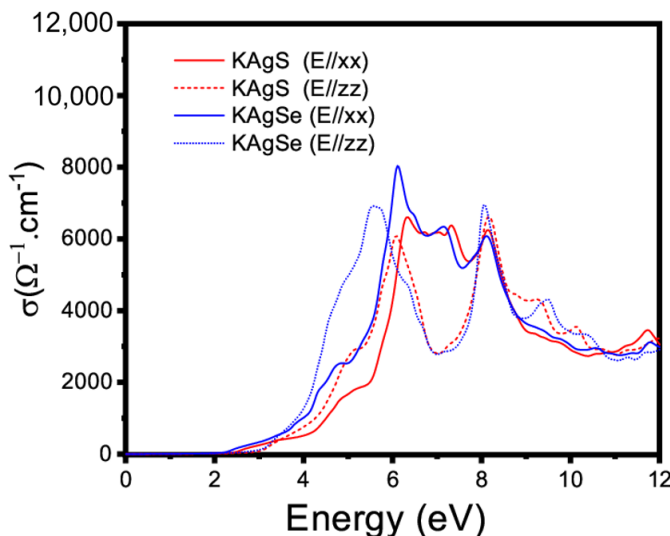


Figure 12. Simulated optical conductivity $\sigma(\omega)$ of KAgS and KAgSe.

3.4.2. Nonlinear Optical Parameters

The nonlinearity in optical material occurs when the medium interacts with an intense electromagnetic field, leading to the second and third harmonic effect. The nonlinear refractive index (n_2) and the third-order nonlinear optical susceptibility ($\chi^{(3)}$) can be estimated using generalized Miller's rule:

$$\chi^{(3)} = \frac{A}{(4\pi)^4} \left(\frac{E_d}{E_0} \right)^4 \quad (7)$$

$$n_2 = \frac{12\pi\chi^{(3)}}{n(0)} \quad (8)$$

where the constant A is equal to 1.7×10^{-10} esu [66] and E_0 and E_d are the dispersion parameters presented above in Table 2. The estimated values of n_2 and $\chi^{(3)}$ are summarized in Table 3. All simulated parameters are in the same range as the other materials used in nonlinear optics applications [67,68]. The results presented in Table 3 reveal the highest value of nonlinear optical parameters in KAgSe compounds for the z polarization direction, suggesting that this compound is promising for nonlinear optical devices.

Table 3. Nonlinear optical parameters: nonlinear refractive index n_2 and third-order nonlinear optical susceptibility $\chi^{(3)}$ for KAgS and KAgSe.

Compound	$n_2 10^{-11}$ esu (E//x)	$n_2 10^{-11}$ esu (E//z)	$\chi^{(3)} 10^{-13}$ esu (E//x)	$\chi^{(3)} 10^{-13}$ esu (E//z)
KAgS	1.37	1.39	7.51	7.62
KAgSe	2.75	3.09	16.2	18.5

4. Conclusions

Overall, we have determined the structural, linear, and nonlinear optical coefficients, as well as the electronic structure, of KAgCh ($Ch = S, Se$), by employing density functional theory as embedded in Wein2k code. The estimated lattice parameters are in close agreement with earlier experimental and theoretical reports. The computed bandgap values for KAgS and KAgSe are 2.57 and 2.39 eV, respectively, which are higher than those reported for many other comparable NLO compounds. The phonon dispersion spectrum predicts the dynamical stability of the studied KAgCh ($Ch = S, Se$). Additionally, the computed refractive indices for KAgCh ($Ch = S, Se$) are quite similar to their equivalent experimental values. We also determined the nonlinear refractive index (n_2) and the third-order nonlinear optical susceptibility ($\chi^{(3)}$) for KAgCh ($Ch = S, Se$). The computed parameters agree well with the experimental and theoretical reports. Both KAgS and KAgSe compounds have good second-order NLO coefficients, large bandgap values, and acceptable optical birefringence, making them suitable candidates for NLO applications.

Author Contributions: Conceptualization, D.B., W.O. and S.K.M.; Methodology, T.S., D.B., H.B.A. and S.K.M.; Software, T.S., D.B., M.B., R.K.S., M.M.S. and A.S.; Validation, T.S., D.B., M.B., W.O., H.B.A., R.K.S. and M.M.S.; Formal analysis, T.S., H.B.A., A.S. and S.K.M.; Investigation, D.B., M.B., R.K.S., M.M.S., A.S. and S.K.M.; Resources, T.S., D.B. and W.O.; Data curation, D.B., M.B., W.O., H.B.A., R.K.S., M.M.S. and S.K.M.; Writing—original draft, D.B. and R.K.S.; Writing—review and editing, D.B. and A.S.; Visualization, D.B.; Project administration, M.M.S.; Funding acquisition, M.M.S. and A.S. All authors have read and agreed to the published version of the manuscript.

Funding: This research received no external funding.

Data Availability Statement: The raw/processed data can be made available with reasonable request to the corresponding author.

Acknowledgments: One of the authors (Debidatta Behera) is thankful to Birla Institute of Technology, Ranchi for the award of an institute fellowship.

Conflicts of Interest: The authors declare that they have no known competing financial interest or personal relationships that could have appeared to influence the work reported in this paper.

References

- Pan, S.; Smit, J.P.; Watkins, B.; Marvel, M.R.; Stern, C.L.; Poeppelmeier, K.R. Synthesis, crystal structure, and nonlinear optical properties of Li₆CuB₄O₁₀: A congruently melting compound with isolated [CuB₄O₁₀] 6-units. *J. Am. Chem. Soc.* **2006**, *128*, 11631–11634. [[CrossRef](#)] [[PubMed](#)]
- Choyke, S.J.; Blau, S.M.; Larner, A.A.; Sarjeant, A.N.; Yeon, J.; Halasyamani, P.S.; Norquist, A.J. Noncentrosymmetry in new templated gallium fluorophosphates. *Inorg. Chem.* **2009**, *48*, 11277–11282. [[CrossRef](#)] [[PubMed](#)]
- Zhang, W.-L.; Cheng, W.-D.; Zhang, H.; Geng, L.; Lin, C.-S.; He, Z.-Z. A strong second-harmonic generation material Cd₄BiO (BO₃)₃ originating from 3-chromophore asymmetric structures. *J. Am. Chem. Soc.* **2010**, *132*, 1508–1509. [[CrossRef](#)] [[PubMed](#)]
- Sun, C.-F.; Hu, C.-L.; Xu, X.; Yang, B.-P.; Mao, J.-G. Explorations of new second-order nonlinear optical materials in the potassium vanadyl iodate system. *J. Am. Chem. Soc.* **2011**, *133*, 5561–5572. [[CrossRef](#)]
- Medhekar, S.; Sarkar, R.K. All-optical passive transistor. *Opt. Lett.* **2005**, *30*, 887–889. [[CrossRef](#)]
- Sarkar, R.K.; Medhekar, S. Passive, “self-trapped family” all-optical half adder using all-optical XOR and AND gates. *Czechoslov. J. Phys.* **2006**, *56*, 359–366. [[CrossRef](#)]
- Atuchin, V.V.; Bazarov, B.G.; Gavrilova, T.A.; Grossman, V.G.; Molokeev, M.S.; Bazarova, Z.G. Preparation and structural properties of nonlinear optical borates K₂(1-x)Rb₂xAl₂B₂O₇, 0 < x < 0.75. *J. Alloy. Compd.* **2012**, *515*, 119–122.
- Tran, T.T.; Koocher, N.Z.; Rondinelli, J.M.; Halasyamani, P.S. Beryllium-free β -Rb₂Al₂B₂O₇ as a possible deep-ultraviolet nonlinear optical material replacement for KBe₂BO₃F₂. *Angew. Chem.* **2017**, *129*, 3015–3019. [[CrossRef](#)]
- Feng, J.; Hu, C.; Xu, X.; Li, B.; Zhang, M.; Mao, J. AgGa₂PS₆: A New Mid-Infrared Nonlinear Optical Material with a High Laser Damage Threshold and a Large Second Harmonic Generation Response. *Chem. Eur. J.* **2017**, *23*, 10978–10982. [[CrossRef](#)]
- Behera, D.; Sharma, R.; Ullah, H.; Waheed, H.S.; Mukherjee, S.K. Electronic, optical, and thermoelectric investigations of Zintl phase AAg₂Se₂ (A = Sr, Ba) compounds: A first principles approach. *J. Solid State Chem.* **2022**, *312*, 123259. [[CrossRef](#)]
- Jain, A.; Ong, S.P.; Hautier, G.; Chen, W.; Richards, W.D.; Dacek, S.; Cholia, S.; Gunter, D.; Skinner, D.; Ceder, G. Commentary: The Materials Project: A materials genome approach to accelerating materials innovation. *APL Mater.* **2013**, *1*, 11002. [[CrossRef](#)]
- Wang, Q.; Li, J.; Liang, Y.; Nie, Y.; Wang, B. KAgSe: A new two-dimensional efficient photovoltaic material with layer-independent behaviors. *ACS Appl. Mater. Interfaces* **2018**, *10*, 41670–41677. [[CrossRef](#)] [[PubMed](#)]

13. Savelberg, G.; Schäfer, H. Beiträge zu den Stabilitätskriterien des PbFCl-typs: Darstellung und Struktur von KAgSe. *J. Less Common Met.* **1981**, *80*, P59–P69. [[CrossRef](#)]
14. Ding, L.-J.; Li, G.-G.; Zhang, C.-W.; Li, P.; Wang, P.-J. Novel two-dimensional KAB ($A = Cu, Au$, $B = S, Se$) photoelectric materials with Prominent carrier mobility and optical properties. *Superlattices Microstruct.* **2021**, *149*, 106773. [[CrossRef](#)]
15. Boualleg, M.; Bennecer, B.; Kalarasse, F. Ab initio predictions of structures and physical properties of the KCuX ($X = Se$ and Te) phases under pressure. *Comput. Condens. Matter* **2022**, *30*, e00616. [[CrossRef](#)]
16. Savelberg, G. Ternäre pnictide und chalkogenide von alkalimetallen und IB-bzw. IIB-elementen/On ternary pnictides and chalkogenides of alkaline metals and IB-resp. II B-elements. *Z. Naturforsch. B* **1978**, *33*, 370–373. [[CrossRef](#)]
17. Mahmoud, M.; Rugut, E.K.; Molepo, M.P.; Joubert, D.P. First-principles study of structural stability, electronic properties and lattice thermal conductivity of KAgX ($X = S, Se, Te$). *Eur. Phys. J. B* **2019**, *92*, 1–10. [[CrossRef](#)]
18. Basri, S.; Zulkifli, M.E.; Hazri, N.S.; Kamarudin, S.K. Quantum Behaviour of Mg and Mg-Al-Zn Microstructure. *Crystals* **2023**, *13*, 501. [[CrossRef](#)]
19. Mounet, N.; Gibertini, M.; Schwaller, P.; Campi, D.; Merkys, A.; Marrazzo, A.; Sohier, T.; Castelli, I.E.; Cepellotti, A.; Pizzi, G. Two-dimensional materials from high-throughput computational exfoliation of experimentally known compounds. *Nat. Nanotechnol.* **2018**, *13*, 246–252. [[CrossRef](#)]
20. Xu, W.; Wang, R.; Zheng, B.; Wu, X.; Xu, H. New family of two-dimensional ternary photoelectric materials. *ACS Appl. Mater. Interfaces* **2019**, *11*, 14457–14462. [[CrossRef](#)]
21. Zhu, X.-L.; Yang, H.; Zhou, W.-X.; Wang, B.; Xu, N.; Xie, G. KAgX ($X = S, Se$): High-performance layered thermoelectric materials for medium-temperature applications. *ACS Appl. Mater. Interfaces* **2020**, *12*, 36102–36109. [[CrossRef](#)] [[PubMed](#)]
22. Wang, Q.; Liang, Y.; Yao, H.; Li, J.; Wang, B.; Wang, J. Emerging negative differential resistance effects and novel tunable electronic behaviors of the broken-gap KAgSe/SiC 2 van der Waals heterojunction. *J. Mater. Chem. C* **2020**, *8*, 8107–8119. [[CrossRef](#)]
23. Konar, S.; Biswas, A. Soliton-soliton interaction with Kerr law nonlinearity. *J. Electromagn. Waves Appl.* **2005**, *19*, 1443–1453. [[CrossRef](#)]
24. Medhekar, S.; Sarkar, R.K.; Paltani, P.P. Coupled spatial-soliton pairs in saturable nonlinear media. *Opt. Lett.* **2006**, *31*, 77–79. [[CrossRef](#)]
25. Khalique, C.M.; Biswas, A. Optical solitons with parabolic and dual-power law nonlinearity via Lie symmetry analysis. *J. Electromagn. Waves Appl.* **2009**, *23*, 963–973. [[CrossRef](#)]
26. Sarkar, R.K.; Medhekar, S. Spatial soliton pairing of two cylindrical beams in saturable nonlinear media. *Prog. Electromagn. Res. M* **2009**, *9*, 53–64. [[CrossRef](#)]
27. Biswas, A.; Yıldırım, Y.; Yaşar, E.; Zhou, Q.; Alshomrani, A.S.; Belic, M. Optical soliton perturbation in parabolic law medium having weak non-local nonlinearity by a couple of strategic integration architectures. *Results Phys.* **2019**, *13*, 102334. [[CrossRef](#)]
28. Medhekar, S.; Sarkar, R.K.; Paltani, P.P. Soliton pairing of two coaxially co-propagating mutually incoherent 1-D beams in Kerr type media. *Opt. Appl.* **2007**, *37*, 243.
29. Biswas, A.; Kara, A.H.; Khan, S.; Yildirim, Y.; Mahmood, M.F.; Alshehri, H.M.; Belic, M.R. Conservation laws for cubic-quartic optical solitons with complex Ginzburg–Landau equation having five nonlinear refractive index structures. *Adv. Mater. Rapid Commun.* **2022**, *16*, 137–141.
30. Shwetanshumala, S.; Konar, S. Bright optical spatial solitons in a photorefractive waveguide. *Phys. Scr.* **2010**, *82*, 45404. [[CrossRef](#)]
31. Biswas, A.; Sonmezoglu, A.; Ekici, M.; Alzahrani, A.K.; Belic, M.R. Cubic-quartic optical solitons with differential group delay for Kudryashov's model by extended trial function. *J. Commun. Technol. Electron.* **2020**, *65*, 1384–1398. [[CrossRef](#)]
32. Sarkar, R.K.; Medhekar, S. Mutual-focusing of two co-propagating beams and formation of trapped spatial breather pair in saturable nonlinear media. *Optik* **2010**, *121*, 339–346. [[CrossRef](#)]
33. Blaha, P.; Schwarz, K.; Madsen, G.; Kvasnicka, D.; Luitz, J. Inst. F. Mater. Chem. TU Vienna. Available online: <http://susy.theochem.tuwien.ac.at> (accessed on 19 April 2023).
34. Hafner, J. Ab-initio simulations of materials using VASP: Density-functional theory and beyond. *J. Comput. Chem.* **2008**, *29*, 2044–2078. [[CrossRef](#)] [[PubMed](#)]
35. Hohenberg, P.; Kohn, W. Density functional theory (DFT). *Phys. Rev.* **1964**, *136*, B864. [[CrossRef](#)]
36. Blaha, P.; Schwarz, K.; Sorantin, P.; Trickey, S.B. Full-potential, linearized augmented plane wave programs for crystalline systems. *Comput. Phys. Commun.* **1990**, *59*, 399–415. [[CrossRef](#)]
37. Perdew, J.P.; Burke, K.; Ernzerhof, M. Generalized gradient approximation made simple. *Phys. Rev. Lett.* **1996**, *77*, 3865. [[CrossRef](#)] [[PubMed](#)]
38. Koller, D.; Tran, F.; Blaha, P. Improving the modified Becke-Johnson exchange potential. *Phys. Rev. B* **2012**, *85*, 155109. [[CrossRef](#)]
39. Behera, D.; Manzoor, M.; Iqbal, M.W.; Lakra, S.; Mukherjee, S.K. Revealing Excellent Electronic, Optical, and Thermoelectric Behavior of EU Based EuAg₂y₂ ($Y = S/Se$): For Solar Cell Applications. *Comput. Condens. Matter* **2022**, *32*, e00723. [[CrossRef](#)]
40. Behera, D.; Mukherjee, S.K. Optoelectronics and Transport Phenomena in Rb₂InBiX₆ ($X = Cl, Br$) Compounds for Renewable Energy Applications: A DFT Insight. *Chemistry* **2022**, *4*, 1044–1059. [[CrossRef](#)]
41. Behera, D.; Mukherjee, S.K. Theoretical Investigation of the Lead-free K₂InBiX₆ ($X = Cl, Br$) Double Perovskite Compounds Using First Principle Calculation. *JETP Lett.* **2022**, *116*, 1–10. [[CrossRef](#)]

42. Otero-de-la-Roza, A.; Luaña, V. Gibbs2: A new version of the quasi-harmonic model code. I. Robust treatment of the static data. *Comput. Phys. Commun.* **2011**, *182*, 1708–1720. [[CrossRef](#)]
43. Hafner, J.; Kresse, G. The vienna ab-initio simulation program VASP: An efficient and versatile tool for studying the structural, dynamic, and electronic properties of materials. In *Properties of Complex Inorganic Solids*; Springer: Berlin/Heidelberg, Germany, 1997; pp. 69–82.
44. Saal, J.E.; Kirklin, S.; Aykol, M.; Meredig, B.; Wolverton, C. Materials design and discovery with high-throughput density functional theory: The open quantum materials database (OQMD). *JOM* **2013**, *65*, 1501–1509. [[CrossRef](#)]
45. Manzoor, M.; Behera, D.; Sharma, R.; Iqbal, M.W.; Mukherjee, S.K.; Khenata, R.; Alarfaji, S.S.; Alzahrani, H.A. Investigation of the structural, mechanical, optoelectronic and, thermoelectric characteristics of cubic GeTiO₃: An ab initio study. *Mater. Today Commun.* **2023**, *34*, 105053. [[CrossRef](#)]
46. Behera, D.; Manzoor, M.; Maharana, M.; Iqbal, M.W.; Zahid, T.; Lakra, S.; Mukherjee, S.K.; Alarfaji, S.S. Structural, electronic, optical, and thermoelectric response of zintl phase AAg₂S₂ (A = Sr/Ba) compounds for renewable energy applications. *Phys. B Condens. Matter* **2023**, *649*, 414446. [[CrossRef](#)]
47. Manzoor, M.; Chowdhury, S.; Sharma, R.; Iqbal, M.W.; Mukherjee, S.K.; Alarfaji, S.S.; Alzahrani, H.A. Insight on the lattice dynamics, thermodynamic and thermoelectric properties of CdYF₃ perovskite: A DFT study. *Comput. Theor. Chem.* **2022**, *113928*. [[CrossRef](#)]
48. Abraham, J.A.; Behera, D.; Kumari, K.; Srivastava, A.; Sharma, R.; Mukherjee, S.K. A comprehensive DFT analysis on structural, electronic, optical, thermoelectric, SLME properties of new Double Perovskite Oxide Pb₂ScBiO₆. *Chem. Phys. Lett.* **2022**, *806*, 139987. [[CrossRef](#)]
49. Behera, D.; Mukherjee, S.K. Structural, elastic, electronic and thermoelectric properties of K₂GeBr₆: A first principle approach. *Mater. Today Proc.* **2023**. [[CrossRef](#)]
50. Koller, D.; Tran, F.; Blaha, P. Merits and limits of the modified Becke-Johnson exchange potential. *Phys. Rev. B* **2011**, *83*, 195134. [[CrossRef](#)]
51. Rubel, O.; Tran, F.; Rocquefelte, X.; Blaha, P. Perturbation approach to ab initio effective mass calculations. *Comput. Phys. Commun.* **2021**, *261*, 107648. [[CrossRef](#)]
52. Behera, D.; Abraham, J.A.; Sharma, R.; Mukerjee, S.K.; Jain, E. First Principles Study of New d0 Half-Metallic Ferromagnetism in CsBaC Ternary Half-Heusler Alloy. *J. Supercond. Nov. Magn.* **2022**, *35*, 3431–3437. [[CrossRef](#)]
53. Behera, D.; Dixit, A.; Nahak, B.; Srivastava, A.; Dubey, S.; Sharma, R.; Mishra, A.K.; Mukherjee, S.K. Structural, electronic, elastic, vibrational and thermodynamic properties of antiperovskites Mg₃NX (X = Ge, Sn): A DFT study. *Phys. Lett. A* **2022**, *453*, 128478. [[CrossRef](#)]
54. Fitzgerel, R.K.; Verhoek, F.H. The law of Dulong and Petit 1960. *J. Chem. Educ.* **1960**, *37*, 545. [[CrossRef](#)]
55. Inaba, H.; Yamamoto, T. Debye temperature of materials. *Netsu Sokutei* **1983**, *10*, 132–145.
56. Behera, D.; Dixit, A.; Kumari, K.; Srivastava, A.; Sharma, R.; Mukherjee, S.K.; Khenata, R.; Boumaza, A.; Bin-Omran, S. Structural, elastic, mechanical, and thermodynamic characteristic of NaReO₃ and KReO₃ perovskite oxides from first principles study. *Eur. Phys. J. Plus* **2022**, *137*, 1345. [[CrossRef](#)]
57. Behera, D.; Manzoor, M.; Sharma, R.; Iqbal, M.W.; Mukherjee, S.K. First principle insight on structural, opto-electronic and transport properties of novel zintl-phase AMg₂Bi₂ (A = Sr, Ba). *J. Solid State Chem.* **2023**, *320*, 123860. [[CrossRef](#)]
58. Ouerghui, W.; Alkhalifah, M.S. Density functional investigation of structural, electronic, optical and thermodynamic properties of Zn_{1-x}BxO semiconductor. *Appl. Phys. A* **2019**, *125*, 1–12. [[CrossRef](#)]
59. Ben Abdallah, H.; Ouerghui, W. Hybrid functional calculations of electro-optical properties of novel Ga_{1-x}In_xTe ternary chalcogenides. *Appl. Phys. A* **2020**, *126*, 1–12. [[CrossRef](#)]
60. Behera, D.; Manzoor, M.; Mukherjee, S.K. Incorporation of Te in enhancing thermoelectric response of AeAg₂SeTe (Ae = Sr, Ba) compounds: A DFT insight. *Comput. Condens. Matter* **2022**, *33*, e00757. [[CrossRef](#)]
61. Joshi, H.; Rai, D.P.; Hnamte, L.; Laref, A.; Thapa, R.K. A theoretical analysis of elastic and optical properties of half Heusler MCoSb (M = Ti, Zr and Hf). *Helijon* **2019**, *5*, e01155. [[CrossRef](#)]
62. Manzoor, M.; Bahera, D.; Sharma, R.; Tufail, F.; Iqbal, M.W.; Mukherjee, S.K. Investigated the structural, optoelectronic, mechanical, and thermoelectric properties of Sr₂TaO₆ (B = Sb, Bi) for solar cell applications. *Int. J. Energy Res.* **2022**, *46*, 23698–23714. [[CrossRef](#)]
63. Ouerghui, W.; Alkhalifah, M.S.; Abdallah, H. Ben DFT calculations on ZnO_{1-x} compounds for optoelectronic applications. *J. Comput. Electron.* **2021**, *20*, 467–479. [[CrossRef](#)]
64. Alkhalifah, M.S.; Ouerghui, W. DFT calculations of optoelectronic properties of cubic $\left(\text{In}_{1-x}\text{Al}_x\right)\text{O}_3$ In_{1-x}Al_xO₃ alloys. *J. Comput. Electron.* **2021**, *20*, 1234–1247. [[CrossRef](#)]
65. Babushkina, E.A.; Belokopytova, L.V.; Grachev, A.M.; Meko, D.M.; Vaganov, E.A. Variation of the hydrological regime of Bele-Shira closed basin in Southern Siberia and its reflection in the radial growth of Larix sibirica. *Reg. Environ. Chang.* **2017**, *17*, 1725–1737. [[CrossRef](#)]
66. Ouerghui, W.; Gassoumi, M.; Beji, L.; Maaref, M.A. Optical properties of quaternary GaMnAsP thin layer grown by molecular beam epitaxy. *Phys. E Low-Dimens. Syst. Nanostructures* **2021**, *131*, 114733. [[CrossRef](#)]

67. Msalmi, R.; Elleuch, S.; Hamdi, B.; Zouari, R.; Naili, H. Synthesis, DFT calculations, intermolecular interactions and third order nonlinear optical properties of new organoammonium tetrabromocadmite (II):(C₅H₆N₂Cl)₂[CdBr₄]·H₂O. *J. Mol. Struct.* **2020**, *1222*, 128853. [[CrossRef](#)]
68. Sharda, S.; Sharma, N.; Sharma, P.; Sharma, V. New quaternary Sb-Se-Ge-In chalcogenide glasses: Linear and nonlinear optical properties. *J. Electron. Mater.* **2013**, *42*, 3367–3372. [[CrossRef](#)]

Disclaimer/Publisher's Note: The statements, opinions and data contained in all publications are solely those of the individual author(s) and contributor(s) and not of MDPI and/or the editor(s). MDPI and/or the editor(s) disclaim responsibility for any injury to people or property resulting from any ideas, methods, instructions or products referred to in the content.